Desalination 404 (2017) 200–214

Contents lists available at ScienceDirect

Desalination

journal homepage: www.elsevier.com/locate/desal

Energy and economic analysis of a hollow fiber membrane-based desalination system driven by solar energy

Li-Zhi Zhang [a,b,*], Guo-Pei Li [a]

[a] Key Laboratory of Enhanced Heat Transfer and Energy Conservation of Education Ministry, School of Chemistry and Chemical Engineering, South China University of Technology, Guangzhou 510640, China
[b] State Key Laboratory of Subtropical Building Science, South China University of Technology, Guangzhou 510640, China

HIGHLIGHTS

- Hollow fiber membrane module is used for water desalination.
- Solar energy is used.
- Optimum ratio of the storage tank volume to solar collector area is about 12 L/m^2.
- The water production cost is about 16.97 \$/m^3.

GRAPHICAL ABSTRACT

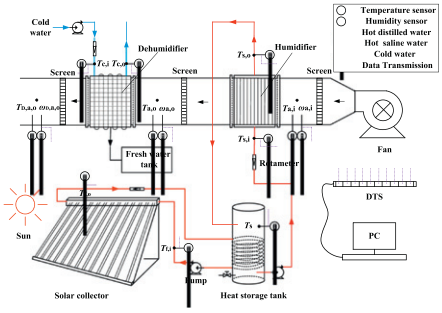

A membrane-based humidification-dehumidification desalination system (MHDD) driven by solar energy.

ARTICLE INFO

Article history:
Received 11 May 2016
Received in revised form 28 October 2016
Accepted 4 November 2016
Available online 18 November 2016

Keywords:
Solar energy
Hollow-fiber membrane
Humidification
Dehumidification
Desalination

ABSTRACT

A novel solar energy driven and membrane-based air humidification-dehumidification desalination (MHDD) system is designed and constructed. To realize a water-salt separation, a hollow fiber membrane module is employed as the humidifier to humidify air with solar energy heated saline water. The humidified air is then cooled and condensed to obtain distilled water. A detailed theoretical model is developed and validated to evaluate the performance of the proposed MHDD system. The whole model includes submodels for the solar collector, the water tank, the membrane humidifier, and the vapor condenser. At a specified membrane area, the effects of the water tank volume and solar collector area on the system performance such as the electric energy consumption for water production (*SEC*), the coefficient of performance (*COP*), etc., are analyzed. The optimal water tank volume and the optimal solar collector area for the desalination system are evaluated. In addition, an economic analysis on the whole system reveals that the system needs a low maintenance cost to make the water production competitive. Generally it provides an attractive alternative to small-scale, stand-alone desalination systems that could provide high purity drinkable water.

© 2016 Elsevier B.V. All rights reserved.

1. Introduction

Global population growth and economic development have resulted in a sharp increase in the demand for fresh water [1]. Water shortage is becoming a worldwide challenge. Although over 71% of the earth's surface is covered with water, about 97.5% of water on the earth is sea or

* Corresponding author at: Key Laboratory of Enhanced Heat Transfer and Energy Conservation of Education Ministry, School of Chemistry and Chemical Engineering, South China University of Technology, Guangzhou 510640, China.
E-mail address: Lzzhang@scut.edu.cn (L.-Z. Zhang).

http://dx.doi.org/10.1016/j.desal.2016.11.002
0011-9164/© 2016 Elsevier B.V. All rights reserved.

brackish water which contains large amounts of salt. As a result, desalination of sea or brackish water becomes the most feasible solution to overcome fresh water shortage. Desalination can be accomplished by a number of techniques [2–10]. Generally, these techniques can be divided into following categories: (1) Thermal processes that involve phase change like Multi-Effect Distillation (MED) [2] and Multi Stage Flash (MSF) [3]. (2) Membrane processes without phase change like Reverse Osmosis (RO) [4,5], Nano Filtration (NF) [6] and Electro Dialysis (ED) [7]. (3) Hybrid processes that involve both phase change and membranes like membrane distillation (MD) [8–10].

Above thermal processes are energy intensive [11,12]. Application of MSF helps the Middle East to hold nearly about 50% of the world's desalination capacity. However, recently with the development of membrane technology, RO desalination method has rapidly been adopted since the 1960s. It now surpasses the thermal processes in new plant installations. At the end of 2009, over 15,000 desalination plants were in operation world-wide, and approximately 50% of those were RO plants [12]. However, reverse osmosis based membrane technology is relied heavily on precious high-pressure mechanical energy. Besides energy intensive, it has maintenance problems [13].

The use of solar energy in desalination represents a promising trend. Because solar thermal energy is a low-grade heat, desalination systems that can be driven by low-grade heat should be searched. In this respect, the solar powered air humidification-dehumidification desalination process is regarded as a favorable technique [14,15]. According to this concept, solar heated sea water is used to humidify the air. The humidified air is then cooled and condensed to produce distilled water. Air humidification can be effectively realized even if the sea water is heated to 60 to 80 °C, so it's a good candidate for solar energy use. There have been many studies of solar energy driven desalination with humidification-dehumidification cycles. Usually packed columns, where the hot sea water and air stream are in a direct contact, are used for air humidification. Farsad et al. [16] studied a solar desalination unit with humidification–dehumidification cycle. A packed tower as a humidifier was used in the system. The heated solution from solar collector is immediately transported to the humidifier and it is in a direct contact with air on the surface of packing. Al-Sulaiman [17] also set up a solar desalination system using humidification-dehumidification processes. The air is humidified through the direct contact with the water in the humidifier. Zhani [18] constructed a plant consisting of a flat plate solar air collector, a flat plate solar water collector, a pad humidifier, an evaporation tower and a condensation tower. For solar powered systems, heat storage is necessary due to the intermittent nature of solar energy heating [19,20]. However the above mentioned studies did not have thermal energy storage devices. Most importantly, all these plants used packed columns to humidify. The coherent problem with direct contact packed columns is that sea water droplets may be carried over to air streams, which would subsequently condensed into the production water. As a result, the purity of the production water would be sacrificed. Another setback of packed columns is that the humidification efficiency is low due to flow maldistribution.

To overcome these problems, this research set up a solar energy driven membrane-based humidification dehumidification desalination system (MHDD). Instead of a packed column a hollow fiber membrane module, in which air is humidified by water through membranes, is used to substitute the packed column. Since water and air stream are separated by membranes, the problem of water droplets crossover is thus solved. Besides, a water tank is used to storage solar energy, thus the problem from the intermittent nature of solar energy use is overcome. To theoretically investigate the system, a mathematical model of the system is developed. The humidifier, the dehumidifier, the solar collector and the thermal energy storage unit are modeled in detail to analyze the system performance. The optimum sizes of the solar collector and the storage tank for the given membrane module are investigated. An economic analysis on the whole system is also performed to investigate the feasibility.

2. System description and experimental setup

2.1. System description

Based on the membrane type humidification–dehumidification processes, a solar energy powered MHDD system is designed and set up in SCUT. The real photos and the schematic sketch of the system are presented in Figs. 1 and 2 respectively. The system mainly consists of a solar collector (contains 36 U-tube glass evacuated tube solar collectors), a heat storage water tank with a coil heat exchanger inside, a membrane-based humidifier (a hollow fiber membrane module) and a dehumidifier (a fin-and-tube heat exchanger). The solar collector combined with a heat storage tank is employed to capture and store the fluctuant solar energy. In this experiment, NaCl solution with a mass fraction of 3.5% is used to substitute sea water. The collected energy is transferred to the NaCl solution in the tank by the heat transfer media (distilled water) through the coil heat exchanger. The novel cross-flow hollow fiber membrane module developed in our laboratory is used as the humidifier. The fibers are made with modified porous membranes. Composite membranes in the module are composed of two layers: a porous polymer PVDF (polyvinylidene fluoride) layer and a dense PVAL (polyvinyl alcohol) skin layer. The hydrophobic PVDF layer mainly provides the mechanical strength. It also prevents liquid molecules from entering the pores of membranes which has been verified by a long time experiment. Meanwhile the hydrophilic PVAL skin layer provides the permselectivity and improves the permeate flux due to low resistance for moisture transfer. The physical structure, composition and heat and mass transport data of the membrane fibers including membrane thickness (δ_m), fiber outer diameter (d_o), thermal conductivity of membrane (λ_m) and moisture diffusivity in membrane (D_{vm}) are described elsewhere [21] and also listed in Table 2. The heated saline water then flows through the fibers, while the fresh air from a fan flows outside the fibers in the shell side of the module. The surface tension forces between the water and the hydrophobic membrane prevent liquid molecules from entering the pores of membranes. Under trans-membrane vapor partial pressure differences, water vapor from saline water inside the fibers can pass through the pores. It is then absorbed by the air stream outside the fibers. Thus, heat and mass transfer are achieved between the hot saline water and the air streams. Then the saline water flows back to the water tank to be heated again. The heated and humidified air at the exit of the humidifier then passes through the dehumidifier, where it is cooled and the vapor contained is condensed into distilled water. The produced fresh water is collected at the bottom of the dehumidifier and it is stored in the fresh water storage tank.

2.2. Experimental setup

An experimental study is conducted to investigate the feasibility of using solar energy for the MHDD system. The whole system is divided into the outdoor part (a solar collector) and the indoor part (a heat storage water tank and a humidification-dehumidification desalination unit) as shown in Fig. 1.

The solar collector of glass evacuated tube type has high efficiencies compared to flat plate type collectors because it has a highly selective surface coating and a vacuum insulation for the absorber element [22]. U-tube evacuated solar collector as one of the glass evacuated tube solar collectors has the advantages of high-pressure-bearing ability. It can also eliminate the impact of glass evacuated tube cracking caused by frequent cold and hot water alternate shocking, because the water is in U copper tubes instead of in the glass tubes. In view of the above characteristics, a 36 U-tube evacuated solar collector is used in this system, and each collector tube is double-glazed. Between the outer and inner glass, a vacuum jacket is made to eliminate the convective heat losses from the collector to the outside environment. A U copper tube is wedged inside an aluminum fin that is in a close contact with the

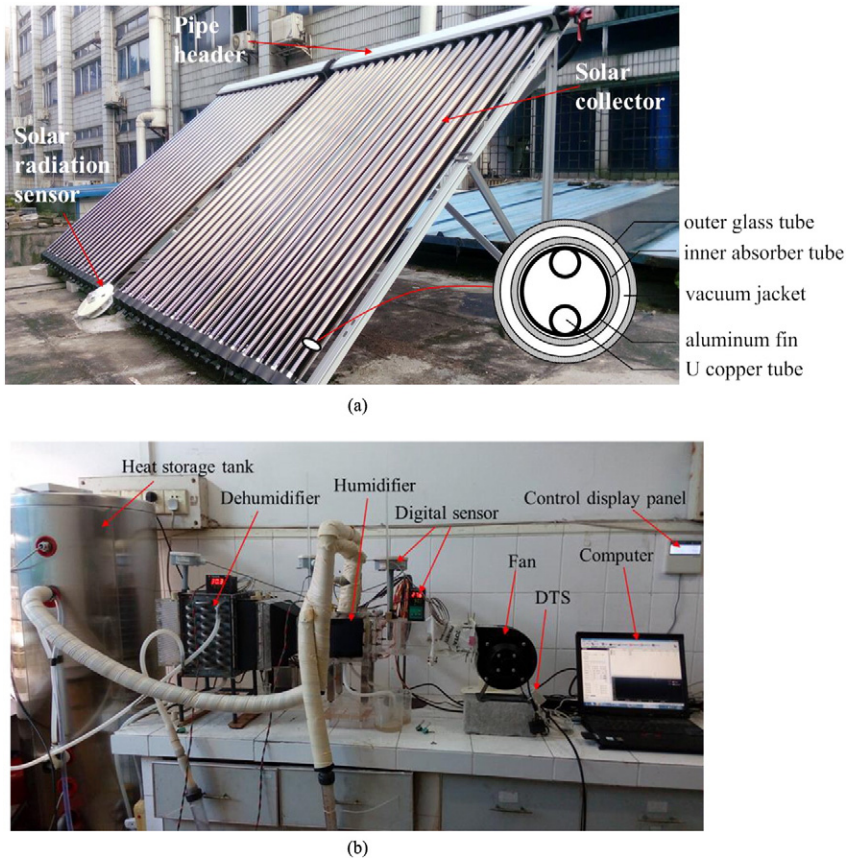

Fig. 1. Real photos of the system. (a) The outdoor part: the solar collector, (b) the indoor part: heat storage tank unit and the humidification-dehumidification desalination system.

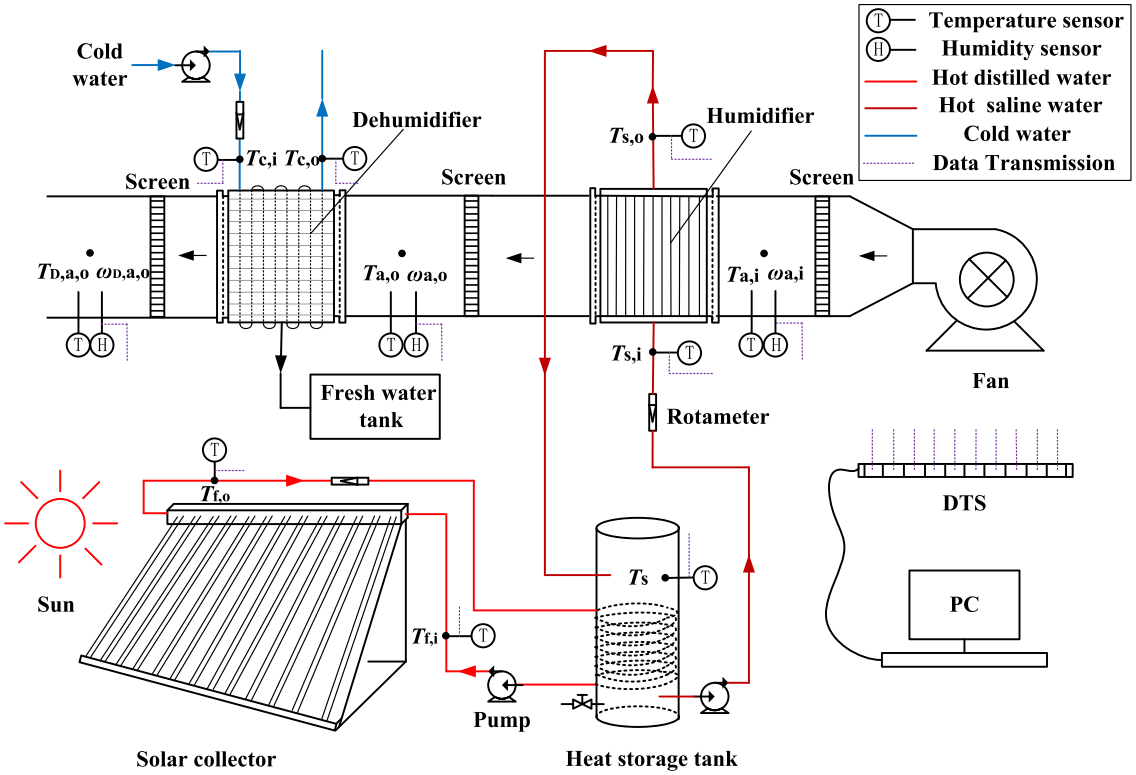

Fig. 2. Schematic diagram of the solar powered membrane-based humidification-dehumidification desalination system (MHDD).

Table 1
Parameters of the solar collector and the heat storage tank for this system.

Material	Parameters	Symbol	Unit	Value
Outer glass tube	Outer diameter	d_o	mm	58
	Thickness	δ_o	mm	2
	Transmissivity	τ	–	0.9
Inner absorber tube	Outer diameter	d_i	mm	47
	Thickness	δ_i	mm	2
	Absorptivity	α	–	0.9
	Effective length	L	m	1.71
	Tube number	n_{col}	–	36
	Effective absorption area	A_e	m^2	4.13
Heat storage tank	Diameter	–	m	0.46
	Height	–	m	1.5
	Capacity	–	L	150
	Heat loss coefficient	U_t		
	W m^{-2} K^{-1}	0.8		
Surface area	A_t	m^2	2.5	
Coil heat exchanger	Outer diameter	–	mm	12
	Thickness	δ	mm	1
	Effective length	L	m	50
	Heat transfer coefficient	U_{coil}		
	W m^{-2} K^{-1}	250		
Heat transfer area	A_{coil}	m^2	1.884	

inner glass tube, as shown in Fig. 1(a). In order to transfer the heat energy between the collector and the saline water inside the tank, a 50 m long coiled tube made of 316L stainless steel is used and placed inside the tank. The outside of the heat storage tank is covered by a 5 cm thick polyurethane foam to insulate heat transfer from the inside to the environment. The inner shell of the tank is made of 304 stainless steel. 304 and 316L stainless steels are used to ensure the equipment are corrosion resistant to saline water. The U-tubes in the evacuated solar collector and the coiled tube in the heat storage tank are filled with distilled water in advance as the heat transport media. Parameters of the solar collector, the heat storage tank and the coil heat exchanger are listed in Table 1. In this system, a hollow fiber membrane module made in our laboratory is used as the humidifier. The detailed illustration of the structure is shown in Fig. 3(a). The production process and the real photo of the module can be found in [23]. The silicone tube is used as distilled water and saline water lines. The membrane module and the saline water lines are covered by PVC (polyvinyl chloride) heat insulation cotton to reduce the heat losses. The dehumidifier is a fin-and-tube heat exchanger. 42 tubes made with 316L stainless steel are mounted by aluminum fins. At the bottom of the dehumidifier, a collecting trough is designed to collect the produced fresh water into

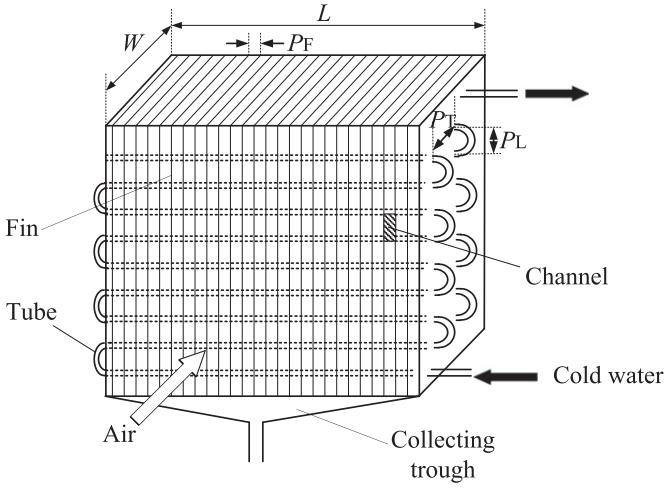

Fig. 4. Schematic diagram of the dehumidifier.

the fresh water storage tank as depicted in Fig. 4. The structure and the physical parameters of the humidifier and the dehumidifier are listed in Table 2. The fin-and-tube heat exchanger is used as the dehumidifier because heat transfer coefficient at the air side is significantly lower than that of solution side. Those aluminum fins provide greater heat transfer areas, improving heat transfer efficiency at the air side. In addition, one 6 W corrosion resistant magnetic circulating pump is used to transport the hot solution to the humidifier. Another one is used to transport the cold water (substitute sea water) to the dehumidifier. A centrifugal fan with frequency conversion governor is used to supply various air volumes for the system. A control display panel is used to display the water temperature at inlet and outlet of the collector. A Data Transmission System (DTS) is used to collect temperature and humidity data of the fluids. They are then transferred to a computer. Several screens are placed inside and along the air duct to uniformly distribute the air stream. In order to maintain constant inlet air states, the indoor part of the system is installed in an air-conditioned room whose temperature and humidity conditions are set to the typical local weather conditions.

2.3. Measurement devices

In order to evaluate the system performance, several key parameters are to be measured such as, flow rates of air and solution streams,

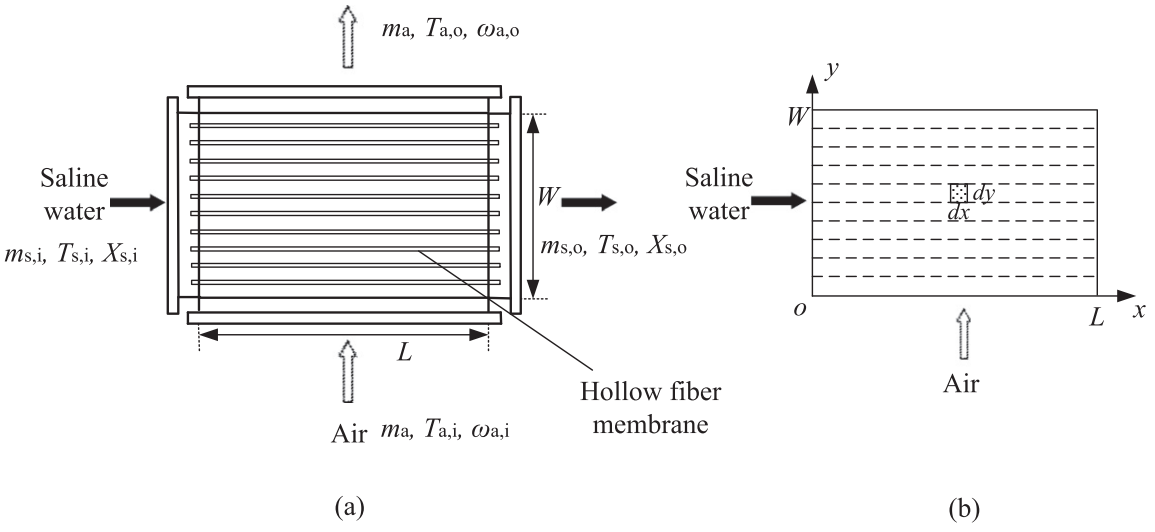

Fig. 3. Schematic of the hollow fiber membrane humidifier: (a) The illustration of structure of module; (b) Schematic diagram of the model calculation.

Table 2
Physical and transport properties of the humidifier and the dehumidifier under design operating conditions.

Humidifier			Dehumidifier		
Symbol	Unit	Value	Symbol	Unit	Value
L_H	mm	90	L_D	mm	200
W_H	mm	90	W_D	mm	150
H_H	mm	90	H_D	mm	200
n_f	–	1400	P_L	mm	25.4
d_o	mm	1.5	P_T	mm	22.0
d_i	mm	1.3	P_F	mm	2.2
A_v	m^2/m^3	814	D_o	mm	9.52
φ	–	0.30	D_i	mm	8.20
N_L	–	40	D_c	mm	10.2
A_{tot}	m^2	0.59	D_h	mm	3.63
δ_m	mm	0.1	N_r	–	6
λ_m	W m^{-1} K^{-1}	0.17	δ_{fin}	mm	0.12
D_{vm}	m^2/s	9×10^{-7}	$A_{p,o}$	m^2	0.25
$Re_{do,max}$	–	113	A_{ff}	m^2	0.021
h_{tot}					
kW m^{-2} K^{-1}	0.0921	A_i	m^2		0.216
k_{tot}	m/s	0.0073	A_h	m^2	2.95

temperature of solution at inlet and outlet of the humidifier, relative humidity and temperature of air at inlets and outlets of the humidifier and the dehumidifier. Three digital temperature-humidity sensors (AF3485Y) with an accuracy of ±2.5% and a resolution of 0.1% are used to measure the temperature and relative humidity of the air. PT100 temperature sensors with an accuracy of ±0.1 °C are used to measure the solution temperature at inlets and outlets of the humidifier and the dehumidifier. All sensors are calibrated before the experiment. Air flow rates are obtained by a hot wire anemometer (TESTO 425) with an accuracy of ±0.15%. To measure the flow rates of water entering the humidifier and the dehumidifier, two rotor-flow meters are used with an accuracy of ±0.5%. A solar radiation sensor (RS232) working in the range from 0 to 2000 W/m^2 with an accuracy of ±2% is used to measure the outdoor solar radiation, which is also transported to the computer. A conductivity meter (DDS-307) combined with a DJS-1 platinum black electrode with an accuracy of ±0.5% is used to measure the electrical conductivity of the produced water.

3. Mathematical modeling

3.1. Evacuated solar collector

The solar collector used in this system consists of 36 U-tube evacuated solar collectors, which are connected in series by the pipe header. A solar radiation sensor placed at the same slope with the collector is used to measure the outdoor solar radiation as shown in Fig. 1(a). To obtain the useful energy collected by the solar collector, the mathematical model is established taking into account the following assumptions:

(1) The energy stored in the collector is negligible.
(2) The flow rate of water inside the collector tube is constant.
(3) In the vacuum jacket, air convective heat loss and heat conduction loss are negligible.
(4) The fluid temperature remains under 100 °C. During the operation time, the fluid has no phase change.
(5) Solar energy absorption by the outer glass is negligible. Only the energy absorbed by the inner absorber glass is considered.

Based on the above assumption, the useful solar energy (q_{solar}) is equal to the energy absorbed (S) minus the heat losses ($q_{loss,c}$) from the collector to the surrounding. It can be obtained from the following formula [24]:

$$q_{solar} = S - q_{loss,c} = F_R\left[I_t \tau\alpha A_e - A_a U_L (T_{f,i} - T_e)\right] \quad (1)$$

The collector heat removal factor (F_R) is the ratio of useful heat obtained in collector to the heat collected by collector, and it can be expressed as:

$$F_R = \frac{m_f c_{pf}}{A_a U_L}\left[1 - \exp\left(-\frac{A_a U_L F'}{m_f c_{pf}}\right)\right] \quad (2)$$

where

$$A_p = n\mathrm{cold}_i L,\ \ A_a = \pi A_p \ \text{ and } \ A_e = 1.43 A_p \quad (3)$$

where, I_t is the global solar radiation, τ is transmissivity of the outer glass, α is absorptivity of the selective absorbing coating, F' is the collector efficiency factor taken as 0.9 for this collector [25]; U_L is the collector overall heat loss coefficient which can be estimated from [25] as $U_L = 0.003(T_{fi} - T_e) + 0.89$; A_p is the projection area of absorber tubes, A_a is outer surface area of absorber tubes, A_e is effective heat absorption area of absorber tubes, T_e is the outside environment temperature, m_f is the flow rate of the distilled water in the tube.

The energy conservation of the distilled water in the solar collectors is written as:

$$q_{solar} = c_{pf} m_f (T_{f,o} - T_{f,i}) \quad (4)$$

where, $T_{f,i}$ and $T_{f,o}$ are the inlet and outlet water temperature to/from the collector respectively.

The instantaneous collector efficiency, η_i, is the ratio of useful energy obtained in the collector to solar radiation to the collector. It can be formulated as:

$$\eta_i = \frac{q_{solar}}{I_t A_e} = F_R \tau\alpha - \frac{F_R A_a U_L}{A_e}\left(\frac{T_{f,i} - T_e}{I_t}\right) \quad (5)$$

3.2. Coil heat exchanger

A coil heat exchanger placed in the heat storage tank is used to transfer the energy collected by the solar collector to the water in the tank, as

shown in Fig. 2. The following equations present the corresponding model:

$$c_{pf} m_f (T_{f,o} - T_{f,i}) = U_{coil} A_{coil} \frac{(\Delta T_2 - \Delta T_1)}{\ln(\Delta T_2 / \Delta T_1)} \quad (6)$$

where, U_{coil} is the overall heat transfer coefficient of the coil in the storage tank, A_{coil} is the heat transfer area of the coil, those structure parameters of the coil heat exchanger can be found in Table 1.

Assuming that the inlet and outlet water temperatures of the coil heat exchanger are equal to the outlet and inlet water temperatures of the solar collector respectively, and then ΔT_2 and ΔT_1 can be written as:

$$\Delta T_2 = T_{f,o} - T_s \text{ and } \Delta T_1 = T_{f,i} - T_s \quad (7)$$

where T_s is the temperature of water in the heat storage tank.

3.3. Heat storage tank

Due to the intermittent nature of solar energy, a thermal energy storage unit (TES) is used in this system. For the energy balance and governing equations of the heat storage tank the following assumptions are considered:

(1) Water tank is a completely mixed storage tank, and the temperature distribution inside the saline water storage tank is homogeneous.
(2) For this well mixed model, solution temperature (T_s) and concentration (X_s) in the tank is equal to the inlet solution temperature ($T_{s,i}$) and concentration ($X_{s,i}$) of the humidifier.
(3) The heat loss coefficient from the tank to the environment is constant.
(4) Since water tank is located indoors, the temperature of the indoor environment is equal to the inlet air temperature to the humidifier ($T_{a,i}$).

In the process of dynamic operation, the water in the tank has a variable level and a variable temperature. The energy balance equation of the storage tank without makeup water is represented as follows:

$$\rho_s c_{ps} \frac{d(T_s V_{tank})}{dt} = q_{solar} - q_{out} - q_{loss,t} \quad (8)$$

where T_s and V_{tank} are the temperature and the volume of water in the heat storage tank. q_{out} is the output heat load:

$$q_{out} = c_{ps} m_{s,i} T_{s,i} - c_{ps} m_{s,o} T_{s,o} \quad (9)$$

where $T_{s,i}$ is the temperature to the humidifier (leaving the tank), and $T_{s,o}$ is the temperature outlet the humidifier (reaching the tank). $m_{s,i}$ and $m_{s,o}$ are the inlet and outlet mass flow rates of the saline water of the humidifier respectively as shown in Fig. 3. Based on mass conservation, $m_{s,o}$ can be written as:

$$m_{s,o} = m_{s,i} - m_a(\omega_{a,o} - \omega_{a,i}) \quad (10)$$

where $\omega_{a,i}$ and $\omega_{a,o}$ are the inlet air humidity and the outlet air humidity of the humidifier respectively. In Eq. (8), $q_{loss,t}$ is the heat loss from the tank to the indoor environment:

$$q_{loss,t} = U_t A_t (T_s - T_{a,i}) \quad (11)$$

3.4. Hollow fiber membrane humidifier

As a separation equipment, the hollow fiber membrane module is a key unit in the system. It is like a cross-flow shell-and-tube heat mass exchanger. Air stream flows in a cross flow manner across the hollow fiber tube bank. The fiber-to-fiber modeling is not likely considering that there are numerous fibers. Therefore a parallel-plates heat mass exchanger modeling as an alternative approach is used in this section. The detail is described in Ref [23]. The convective heat transfer coefficients h (kW m^{-2} K^{-1}) and the convective mass transfer coefficient k (m/s) of solution and air can be represented by Nusselt numbers and Sherwood number respectively as:

$$Nu = \frac{hd}{\lambda} \quad (12)$$

$$Sh = \frac{kd}{D} = \frac{Nu}{Le^{1/3}} \quad (13)$$

where λ is heat conductivity, Le is the Lewis Number. D is diffusivity, which represents D_{ws}, water diffusivity in solution for the tube side, and D_{va}, moisture diffusivity in air for the shell side, respectively.

Since the Re for the air stream and the solution stream (in the fine fibers) are all much less than 2300, both air and solution can be considered to be laminar. For fully developed laminar heat transfer in round tubes:

$$Nu_s = 3.658 \quad (14)$$

Nusselt numbers of air stream are given in [26]:

$$Nu_a = 1.13 C_1 Re_{d_o,max}^{m} Pr_a^{0.33} \quad (15)$$

where the constants C_1 and m can be found in [26], Pr is Prandtl number. $Re_{do,max}$ is calculated by the maximum air stream velocity occurring within the hollow fiber tube bank ($u_{a,max}$):

$$Re_{do,max} = \frac{u_{a,max} d_o}{\nu_a} \quad (16)$$

Overall heat and mass transfer coefficients of the hollow fiber membrane humidifier [27]:

$$\frac{1}{h_{tot}} = \frac{1}{h_s}\left(\frac{d_o}{d_i}\right) + \frac{\delta_m}{\lambda_m}\left(\frac{d_o}{\overline{d}}\right) + \frac{1}{h_a} \quad (17)$$

$$\frac{1}{k_{tot}} = \frac{1}{k_s^e}\left(\frac{d_o}{d_i}\right) + \frac{\delta_m}{D_{vm}}\left(\frac{d_o}{\overline{d}}\right) + \frac{1}{k_a} \quad (18)$$

where ke s is the equivalent moisture transfer coefficient in the solution side, δ_m is membrane thickness, $\overline{d}$ is mean diameter of membrane, D_{vm} is the moisture diffusivity in membrane.

For the air and solution streams, normalized governing equations for heat and moisture conservation are described as follows:

$$\frac{\partial T_a}{\partial y} = \frac{h_{tot} A_{tot}}{m_a c_{pa} W}(T_s - T_a) \quad (19)$$

$$\frac{\partial \omega_a}{\partial y} = \frac{\rho_a k_{tot} A_{tot}}{m_a W}(\omega_s - \omega_a) \quad (20)$$

$$\frac{\partial T_s}{\partial x} = \frac{h_{tot} A_{tot}}{m_s c_{ps} L}(T_a - T_s) + \frac{\rho_a k_{tot} A_{tot} H_w}{m_s c_{ps} L}(\omega_a - \omega_s) \quad (21)$$

$$\frac{\partial X}{\partial x} = \frac{\rho_a k_{tot} A_{tot}}{m_s L}(\omega_s - \omega_a) \quad (22)$$

In equations above-mentioned, x and y are coordinates, X is solution concentration, T is temperature, ω_a is the air humidity, ω_s is the air equilibrium humidity with solution at the temperature T_s and the concentration X_s, H_v is evaporation heat of vapor.

The boundary conditions are given as:

$$x = 0,\ \ T_s = T_{s,i} \quad \omega_s = \omega_{s,i} \tag{23}$$

$$y = 0,\ \ T_a = T_{a,i} \quad \omega_a = \omega_{a,i} \tag{24}$$

where $\omega_{s,i}$ is the air equilibrium humidity with solution at the inlet with a temperature $T_{s,i}$ and a concentration $X_{s,i}$.

The relative humidity (RH) is calculated by humidity (ω) and temperature (T) of the air as [28]:

$$\frac{RH}{\omega} = \frac{e^{5294/T}}{10^6} - 1.61RH \tag{25}$$

Eqs. (19)–(22) are the governing partial differential equations for heat and moisture transfer in the membrane module. Considering that heat and mass transfer are closely coupled in the process, a finite difference method is used to discretize and solve these equations. The

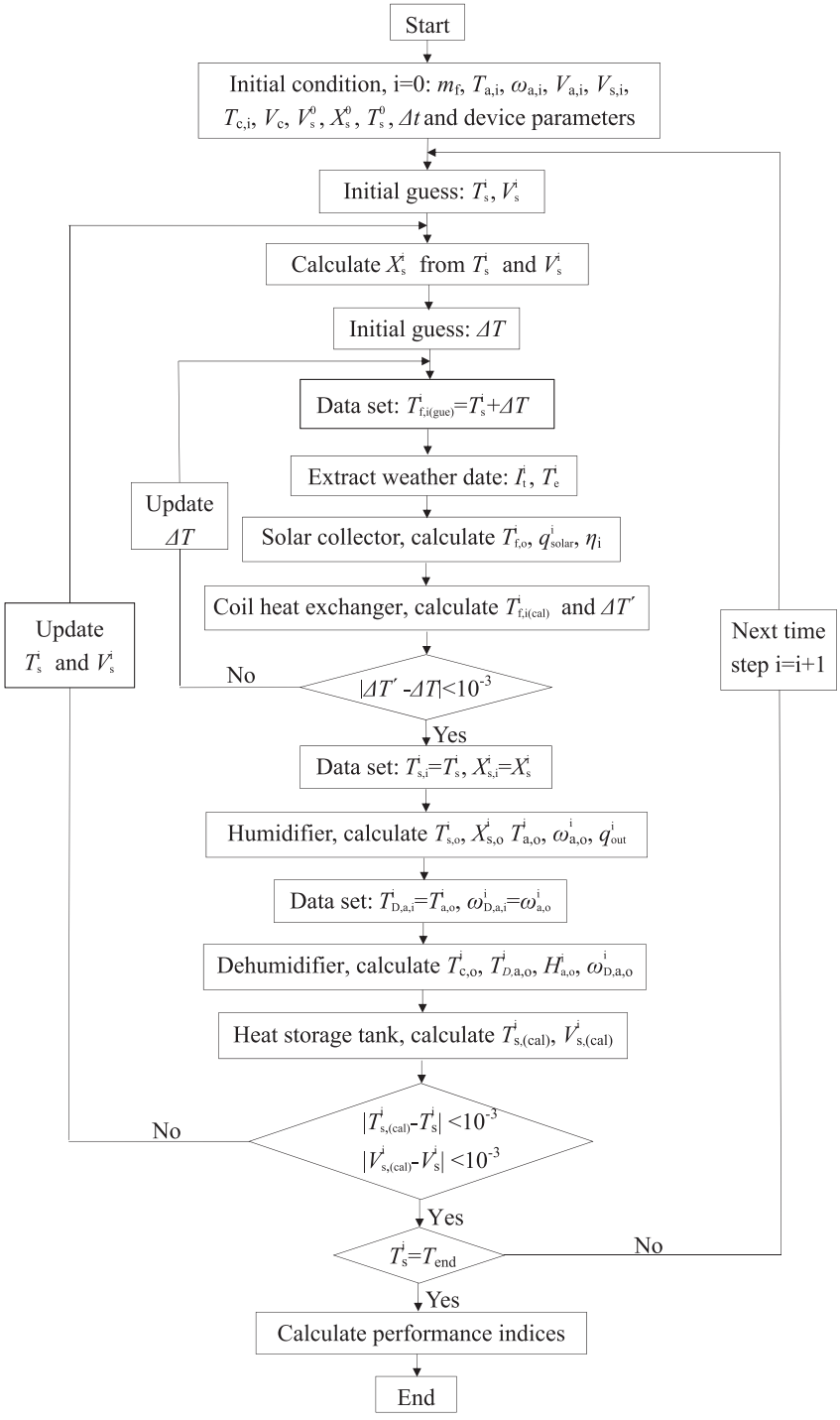

Fig. 5. Flow chart for solution procedure in simulation of the whole system.

schematic diagram of the calculation domain is showed in Fig. 3(b). A grid independence test is done. It can be found that 40 × 40 grids had enough numerical accuracy (less than 0.1%) compared with 50 × 50 grids.

In the shell side of the membrane module, the air stream flows across the hollow fiber tube bank, the pressure drop is:

$$\Delta P_{a,H} = N_L C_2 \frac{\rho_a u_{a,max}^2}{2} f_a \tag{26}$$

In the equation, N_L is the number of fibers along the air stream flow direction, C_2 is a correction factor, f_a is friction factor of air flowing across the tube bank. C_2 and f_a are listed in Ref [26].

For laminar flow in round tubes, solution side pressure drop is:

$$\Delta P_{s,H} = \frac{64}{Re_s}\frac{L_H}{d_i}\frac{\rho_s u_s^2}{2} \tag{27}$$

3.5. Dehumidifier

The dehumidifier is a fin-and-tube heat exchanger as shown in Fig. 4. The effectiveness-Number of Transfer Units (ε-NTU) method is used for this fin-and-tube heat exchanger [29]. The effectiveness can be written as:

$$\varepsilon = 1 - \exp\left\{NTU^{0.22}\left[\exp\left(-C_r NTU^{0.78}\right) - 1\right]/C_r\right\} \tag{28}$$

where

$$NTU = \frac{UA}{m_a c_{pa}} \quad \text{and} \quad C_r = \frac{m_a c_{pa}}{m_c c_{pc}} \tag{29}$$

The total thermal resistance of the heat exchanger can be written as:

$$\frac{1}{UA} = \frac{1}{h_i A_i} + R_w + \frac{1}{\eta_o A_h h_a} \tag{30}$$

The first term of the right-hand-side of Eq. (30) indicates the tube-side thermal resistance, the second term means the tube wall resistance and the last term is the air-side thermal resistance. A_i is the surface area inside the tubes. η_o is fin efficiency, which is available in Ref [26]. A_h is the surface area in hot air side.

In the dehumidifier, solution in the tubes is in single-phase forced convection. The Reynolds numbers for the solution stream are far more than 4000 (about 15,343). For turbulent flow in pipes, the tube-side heat transfer coefficient h_i can be evaluated with the Gnielinski correlation [30]:

$$h_i = \left(\frac{\lambda_i}{D_i}\right)\frac{(Re_{D_i} - 1000)\,Pr(f_i/2)}{1.07 + 12.7\sqrt{f_i/2}\,(Pr^{2/3} - 1)} \tag{31}$$

$$f_i = \left(1.58 \ln Re_{D_i} - 3.28\right)^{-2} \tag{32}$$

where Re_{Di} is Reynolds number based on the inside diameter of the tube, f_i is the friction factor in the tube.

The airside heat transfer characteristics are presented in terms of the Colburn j factor:

$$h_a = j\frac{G_a c_{pa}}{Pr^{2/3}} \tag{33}$$

where G_a is maximum air mass flow rate along air flow direction among fins. j is Colburn j factor, which is a dimensionless heat transfer factor to perform the heat transfer characteristics of air side. Considering the number of tube row (N_r) is six in this dehumidifier, j can be calculated as [31]:

$$j = 0.4 Re_{Dc}^{-0.468 + 0.04076 N_r}\left(\frac{A_o}{A_{p,o}}\right)^{0.159} N_r^{-1.261} \tag{34}$$

where

$$Re_{Dc} = \frac{G_a D_h}{\nu_a \rho_a}, \quad G_a = \frac{m_a}{A_{ff}} \quad \text{and} \quad D_h = \frac{4A_c}{\Pi_c} \tag{35}$$

in Eqs. (34)–(35), A_o is total surface area of the dehumidifier, $A_{p,o}$ is external surface area of tube, A_{ff} is minimum free flow area in the flow channel with fins, D_h is the hydraulic diameter of the air flow channel as showed in Fig. 4, A_c is area of air channel, Π_c is wet perimeter of channel. The detail structure and physical parameters of the dehumidifier are listed in Table 2.

Under dehumidifying conditions, the maximum theoretical heat transfer rate (q_{max}) and the real heat transfer rate (q_{real}) can be written as:

$$q_{max} = \frac{q_{real}}{\varepsilon} = m_a\left(H_{a,i} - H_{c,i}\right) \tag{36}$$

$$q_{real} = m_c c_{pc}\left(T_{c,o} - T_{c,i}\right) = m_a\left(H_{a,i} - H_{a,o}\right) \tag{37}$$

where, $H_{a,i}$ and $H_{a,o}$ are the enthalpy of inlet air and outlet air of the dehumidifier. $H_{c,i}$ is the enthalpy of saturated moist air at the temperature $T_{c,i}$. The outlet air of the dehumidifier is saturated moist air, so the relative humidity of the outlet air is 100%. Then the outlet air temperature ($T_{D,a,o}$) and humidity ($\omega_{D,a,o}$) can be obtained.

In the dehumidifier, the air stream flows across tube bank with fins, the pressure drop is:

$$\Delta P_{a,D} = \frac{G_a^2 V_i}{2}\left[\left(1 + \frac{A_{ff}^2}{A_{fr}^2}\right)\left(\frac{V_o}{V_i} - 1\right) + f\frac{A_o V_m}{A_{ff} V_i}\right] \tag{38}$$

where A_{ff} is minimum free flow area in the flow channel with fins, A_{fr} is the windward area of the dehumidifier, f is friction factor, which is available in Ref [26]. V_i and V_o are the specific volume of the inlet and outlet air ($1/\rho$), V_m is the average of V_i and V_o.

For turbulent flow in round tubes, solution side pressure drop is:

$$\Delta P_{s,D} = f_D\frac{l}{D_i}\frac{\rho_s u_s^2}{2} \tag{39}$$

where f_D is the friction factor in the tube of the dehumidifier.

3.6. Performance indices

To evaluate the performance of the system, several parameters need to be defined.

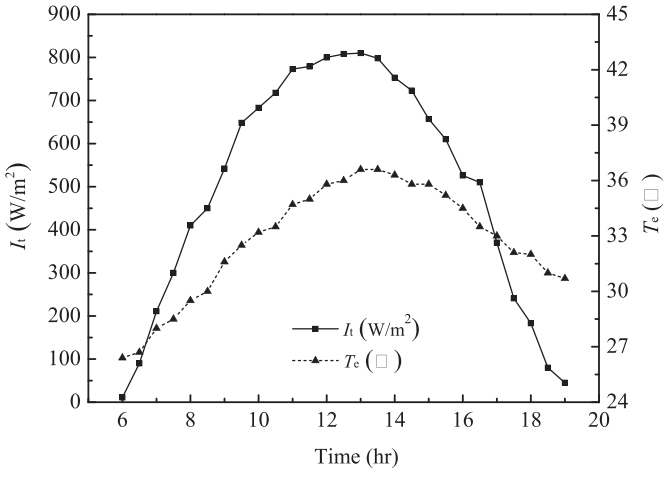

Fig. 6. Measured variations of solar radiation and environment temperature with time on 28 Aug, 2015.

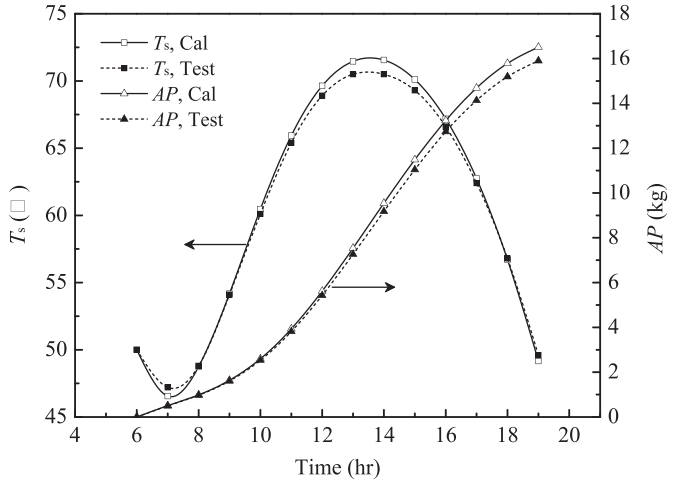

Fig. 7. Calculated (solid lines) and tested (dotted lines) values of the tank water temperature and the accumulated water production during operation time.

Instantaneous freshwater production rates (*IP*) and accumulated water production during the operation period (*AP*) are defined as:

$$IP = m_a(\omega_{D,a,i} - \omega_{D,a,o}) \tag{40}$$

$$AP = \int m_a(\omega_{D,a,i} - \omega_{D,a,o})dt \tag{41}$$

where, $\omega_{D,a,i}$ and $\omega_{D,a,o}$ are the humidity of inlet air and outlet air of the dehumidifier.

Salt rejection was calculated using the following equation:

$$Rj = \left(1 - \frac{\lambda_D}{\lambda_S}\right) \tag{42}$$

where, λ_S and λ_D are the electric conductivity of saline water and distillate respectively.

Specific electric energy consumption for unit volume of water production (*SEC*) is as follow:

$$SEC = \frac{\rho_w \int (W_{pump} + W_{fan})dt}{AP} \tag{43}$$

COP (the coefficient of performance of the whole system) and COP_E (electric *COP*) are defined:

$$COP = \frac{AP \cdot H_w}{\int (q_{solar} + W_{pump} + W_{fan})dt} \tag{44}$$

$$COP_E = \frac{AP \cdot H_w}{\int (W_{pump} + W_{fan})dt} \tag{45}$$

where, H_w is the water latent heat of condensation. W_{pump} and W_{fan} are pump and fan power consumption, which can be written as:

$$W_{pump} = \frac{m_s \Delta P_s}{\rho_s \eta_{pump}} \quad \text{and} \quad W_{fan} = \frac{m_a(\Delta P_{a,H} + \Delta P_{a,D})}{\rho_a \eta_{fan}} \tag{46}$$

where η_{pump} and η_{fan} are pump efficiency and fan efficiency respectively.

3.7. Calculation method

Fig. 5 demonstrates the flow chart of the numerical calculation. The detailed solution procedure is introduced as follows:

(1) Input initial condition. Input the operating parameters like the mass flow rate of the distilled water in the collector tube (m_f); the inlet temperature ($T_{a,i}$), humidity ($\omega_{a,i}$) and volumetric flow rate ($V_{a,i}$) of air to the humidifier; the volumetric flow rates of hot saline water ($V_{s,i}$) and cold water (V_c), and the inlet temperature of cold water ($T_{c,i}$); the volume (V_s^0), the concentration (X_s^0), and the temperature (T_s^0) of saline water in the heat storage tank at the beginning; the device parameters like the humidifier, dehumidifier, solar collector, heat storage tank, etc. The time step (Δt) is 15 s.
(2) Assume initial values for the temperature and volume of the saline water in the heat storage tank (T_s^i, V_s^i).
(3) The saline water concentration (X_s^i) is calculated from the total mass of NaCl and the water volume of the tank (V_s^i) at temperature T_s^i.
(4) Assume an initial temperature difference (ΔT).
(5) Set the inlet water temperature to the collector tube (guessed $T_{f,i(gue)}^i$) as $T_s^i + \Delta T$. Extract weather data like solar radiation and environment temperature and solve Eqs. (1)–(5) for the evacuated solar collector and calculate its outlet water temperature ($T_{f,o}^i$), the useful energy collected by the solar collector (q_{solar}^i) and the collector efficiency (η_i).

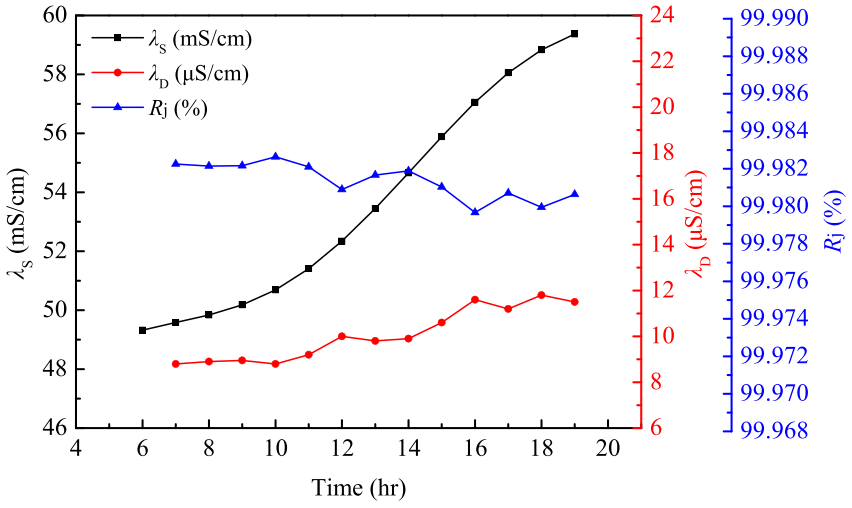

Fig. 8. Variations of the electric conductivity of the saline water and the produced fresh water and the salt rejection during the whole-day operation time.

(6) Solve Eqs. (6)–(7) for the coil heat exchanger and calculate its outlet temperature. This temperature is also the solar collector inlet temperature (calculated $T^{i}_{f,i(cal)}$). Then calculate a new temperature difference ($\Delta T' = T^{i}_{f,i(cal)} - sT^{i}_{s}$). If the deviations between $\Delta T$and ΔT are within the convergence criterion, go to (7); otherwise, let $\Delta T = (\Delta T' + \Delta T)/2$ and return to (5) until convergence criterion is satisfied.

(7) Set the inlet solution temperature ($T^{i}_{s,i}$) and concentration ($X^{i}_{s,i}$) to the humidifier equal to the current solution temperature (T^{i}_{s}) and concentration (X^{i}_{s}) in the heat storage tank. Solve Eqs. (12)–(27) for the humidifier and calculate the outlet temperature ($T^{i}_{s,o}$), concentration ($X^{i}_{s,o}$) of the hot saline water from the humidifier. Calculate the outlet temperature ($T^{i}_{a,o}$), humidity ($\omega^{i}_{a,o}$) of the air from the humidifier. Calculate the output heat load (q^{i}_{out}).

(8) Set the outlet temperature, humidity of the air from the humidifier as the inlet temperature, humidity of the air to the dehumidifier. Solve the Eqs. (28)–(39) for the dehumidifier and calculate the outlet temperature ($T^{i}_{D,a,o}$), humidity ($\omega^{i}_{D,a,o}$) and enthalpy ($H^{i}_{a,o}$) of the air from the dehumidifier. Calculate the outlet temperature of cold water ($T^{i}_{c,o}$) from the dehumidifier.

(9) Solve Eqs. (8)–(11) for the heat storage tank, calculate the temperature ($T^{i}_{s,(cal)}$) and the volume ($V^{i}_{s,(cal)}$) of the saline water in the tank. If the deviations between $T^{i}_{s,(cal)}$ and T^{i}_{s}, $V^{i}_{s,(cal)}$ and V^{i}_{s} are within the convergence criterion, go to (10); otherwise, let $T^{i}_{s} = (T^{i}_{s,(cal)} + T^{i}_{s})/2$ and $V^{i}_{s} = (V^{i}_{s,(cal)} + V^{i}_{s})/2$, then return to (3) until convergence criterion is satisfied.

(10) Go to next time step (i = i + 1) and return to (2) until the required time is reached. Then calculate performance indices.

4. Results and discussion

4.1. Model validation

The validity of the present mathematical model is examined by comparing the simulation results with the experimental results obtained from the test rig. There are many influencing parameters. Optimal operating conditions including the inlet seawater, air flow rates to the humidifier and the packing fractions of the humidifier have been found previously [32]. Those optimal parameters are used in this study. The structural parameters of the humidifier used in this experiment are listed in Table 2. For the size and structure of this humidifier, the inlet hot saline water flow rate is chose at 140 L/h. The flow rate is chose at

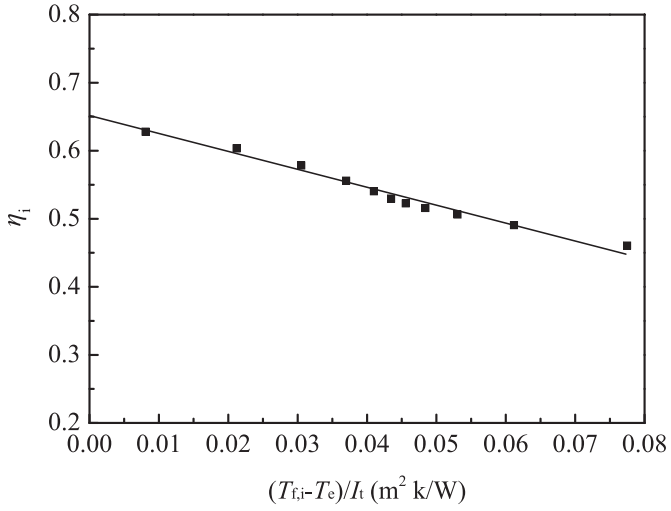

Fig. 9. Efficiencies of the evacuated solar collector.

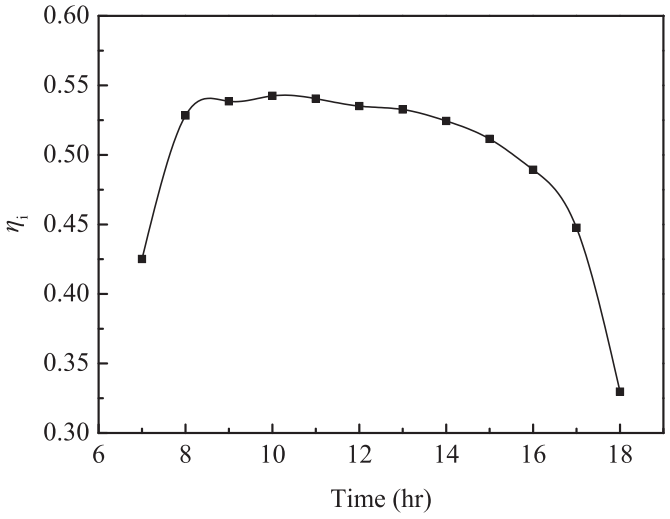

Fig. 10. Variations of the instantaneous collector efficiency with time.

15m^3/h for the inlet air at 35 °C and 65% *RH*. In addition, the initial solution temperature of the tank is set to 50 °C after an overnight insulating, with a concentration 3.5%, and a volume 80 L. The inlet temperature of the cold water is 28 °C (under the condition of room temperature) and cold water flow rate is chose at 160 L/h. The experiments were carried out on 28 Aug., 2015 and the measured operating values of solar radiation and ambient temperature during a day in Guangzhou, China, are shown in Fig. 6. Considering that there is almost no solar radiation before 6 o'clock and after 19 o'clock, the system is operated from 6:00 to 19:00. Based on the above mentioned operating conditions, the calculated and tested values of the tank water temperature (T_s) and the accumulated water production (*AP*) during operation time are given in Fig. 7. As it is shown, the agreements between the calculated and the tested results are good. The relative deviations between the calculated and the tested values of T_s and *AP* are within 1.9% and 4.0% respectively. Therefore the mathematical model is reliable and could be used to study the plant. Furthermore, during the operation, although there is a slight rise, the electric conductivity of the produced fresh water is still basically less than 12 μS/cm, the salt rejection is also stable in the range of 99.978%–99.984%, as showed in Fig. 8. It means that the membrane pore wetting has not occurred and saline water droplets have not

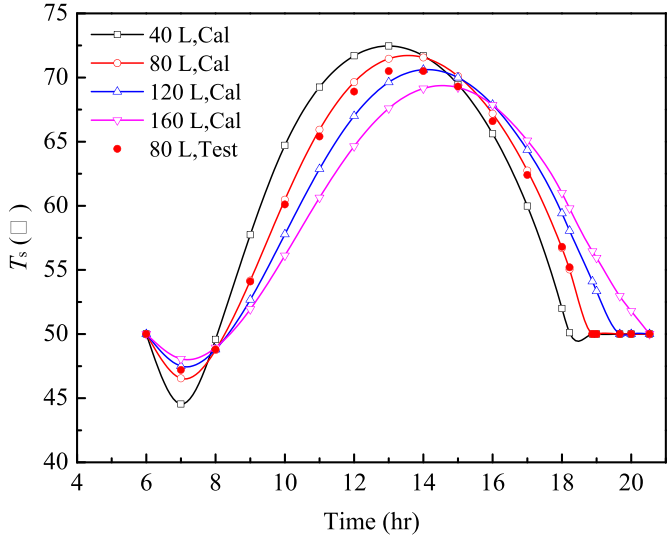

Fig. 11. Effects of water tank volumes on the water temperature in the tank during the operation time.

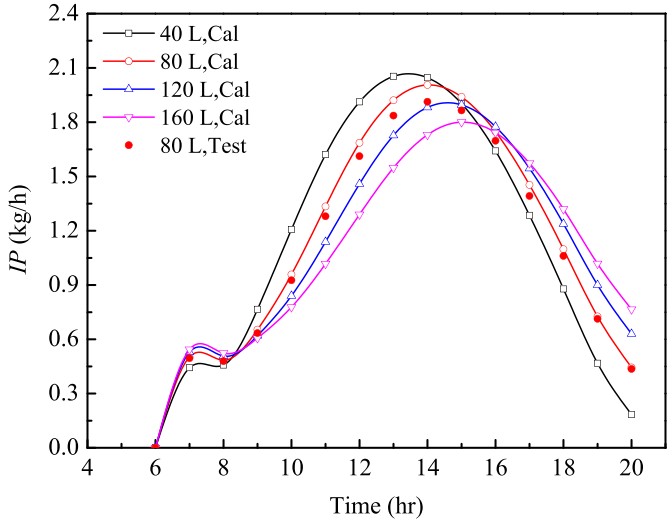

Fig. 12. Effects of water tank volumes on the instantaneous water production rate during the operation time.

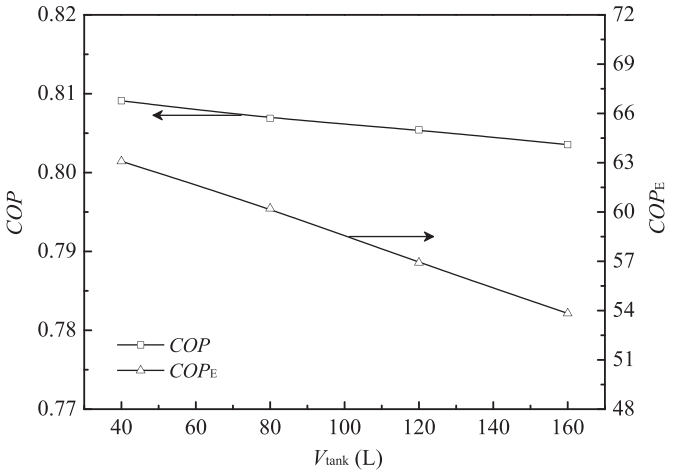

Fig. 14. Variations of *COP* and COP_E with varying water volumes in the tank.

been carried over to air streams, which would subsequently condensed into the production water. Therefore this system is a promising method to obtain high purity water.

4.2. Evacuated solar collector performance

The solar collector is an important component of the solar powered MHDD system. In fact, most of the driving energy for the system is collected by this equipment. So its performance represents a critical factor to the efficiency of the whole system. A measure of its performance is the collection efficiency written in Eq. (5), defined as the radio of the useful energy gain over some specified time period to the incident solar energy. Under above operating conditions, the instantaneous collector efficiencies for the collector with a 4.13 m^2 effective area are illustrated in Fig. 9. The collection efficiency for this collector can be fitted linearly as a function of the parameter $[(T_{f,i} - T_e)/I_t]$:

$$\eta_i = 0.65 - 2.59\left(\frac{T_{f,i} - T_e}{I_t}\right) \quad (47)$$

As shown in Eq. (47), the highest efficiency of the evacuated solar collector can reach 0.65 when the inlet water temperature of the collector is equal to the outside environmental temperature. In general, this U-tube evacuated solar collector has a superior energy-collecting efficiency compared with other plate solar collector or evacuated tube collectors [33,34]. Fig. 10 shows variations of the instantaneous collector efficiency with time during operation time. The collector efficiency varies between 0.33 and 0.55 during the hours of operations and reaches a maximum at about 10:00 am. The reason is that at 10:00 the solar radiation is 683 W/m^2 (about 85% of the noon time value) while the temperature difference between $T_{f,i}$ and T_e is not so large. As a result the ratio of temperature difference to solar radiation reaches a minimum and the collector efficiency attains a maximum.

4.3. Effects of water volumes in the tank

The sizes of the storage tank are simulated. The system with a 50 °C initial saline water temperature is operated from 6:00 until the temperature is below 50 °C in the afternoon. The effective collector area is 4.13m^2 and other operation conditions are all specified as before.

Fig. 11 shows the effects of tank volumes on the water temperature in the tank. The instantaneous water production rate during the operation time is shown in Fig. 12. It is observed that water temperature in the tank fluctuates in response to the daily solar insolation and ambient temperatures. However the water temperature decreases between 6:00

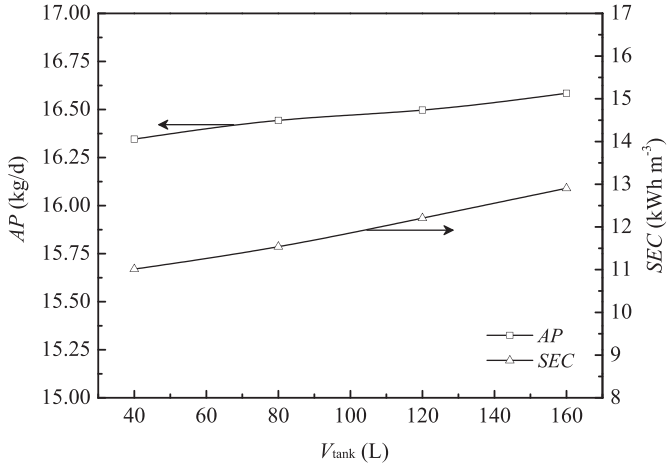

Fig. 13. Variations of the accumulated water production and *SEC* with varying water volumes in the tank.

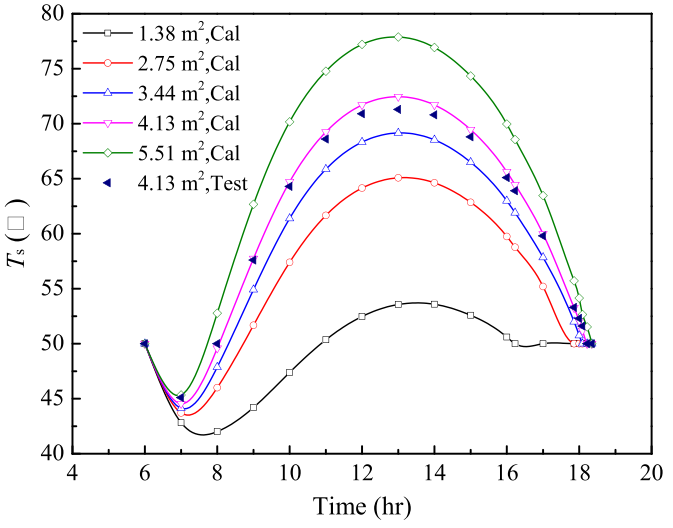

Fig. 15. Effects of collector area on the water temperature in the tank during the operation time.

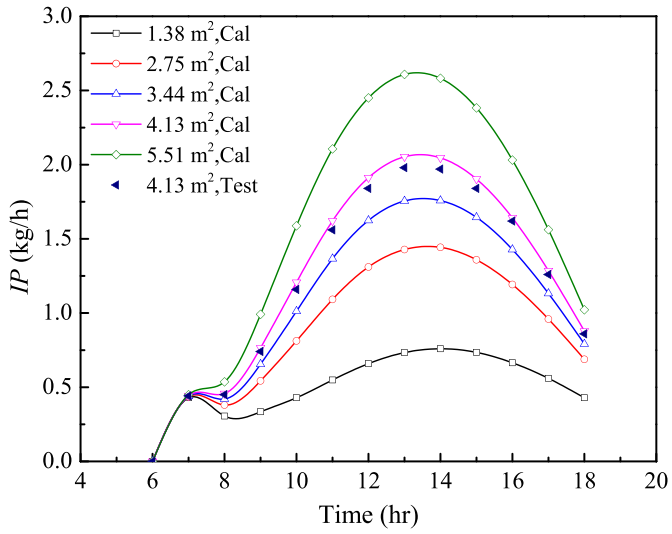

Fig. 16. Effects of collector area on the instantaneous water production rate during the whole-day operation time.

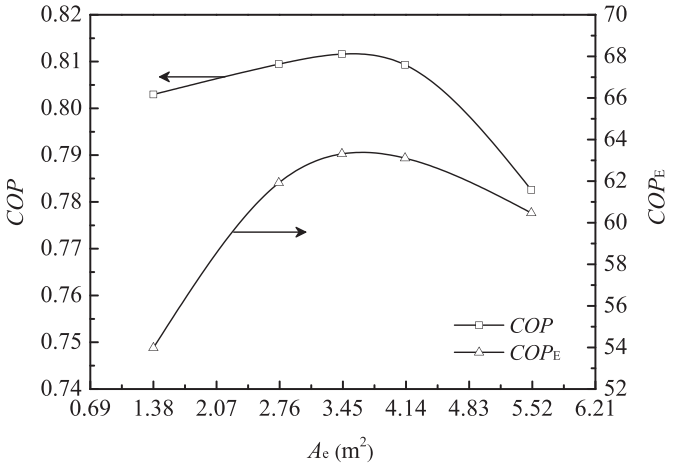

Fig. 18. Variations of *COP* and COP_E with varying collector areas.

and 7:00 because during this period the solar radiation is not strong enough to meet the system demand. The fall in water temperature also results in a reduction in the instantaneous water production rate during 7:00–8:00 as shown in Fig. 12. The water tank temperature reaches a maximum value from 13:00 to 15:00. The instantaneous water production rate also reaches a maximum after half an hour delay. Compared to the tanks of small volumes, water temperature in a big volume tank responds slowly to the daily solar insolation. Therefore, a big volume water tank can store more sensible heat from the intense radiations at noon and it can then supply enough energy for the system operation when the sunlight is weak. In this way, the running time of the system with a 160 L volume tank has an extension of 2.31 h from that with a 40 L volume tank. The system can still run even without solar energy input (after 19:00) as shown in Fig. 11.

The accumulated water production and *SEC* with varying water volumes in the tank are plotted in Fig. 13. The Variations of *COP* and COP_E are plotted in Fig. 14. The systems stop running when the water temperature is below 50 °C in the afternoon. As seen, though the system with a 160 L water volume has a longer running time than that with a 40 L water volume, the accumulated water production is only increased by 1.5%. Longer running time means more electric energy consumption. Therefore with the increase in water volume in the tank, the *SEC* increases and COP_E falls gradually as shown in Figs. 13 and 14. Since a greater volume of water tank has a lower average water temperature throughout the day, and a longer running time, consequently more solar energy is used. In contrast, a weak *AP* increase results in a diminished *COP*. It can be concluded that on the one hand, a larger water tank would be able to reduce the impact of fluctuating solar energy and to store sufficient amount of heat to drive the desalination system when the light is weak. On the other hand there are no further benefits to increase the water tank volume above 40 L. The hollow fiber membrane module is specified at an area of 0.59 m^2.

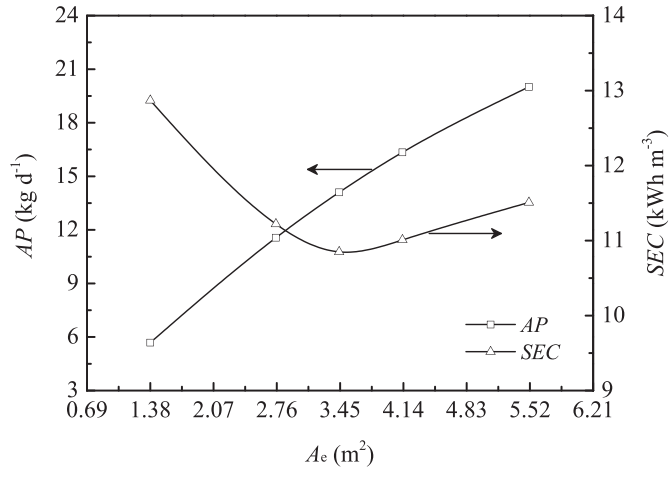

Fig. 17. Variations of the accumulated water production and *SEC* with varying collector areas.

4.4. Effects of solar collector areas

Solar collector is the most important component of the solar heating system. Usually the collector is the most expensive member for the solar desalination system. So it is necessary to search the optimal value of collector area for the system. In this section, the water volume in the tank is set to 40 L and other operating conditions are set as before. Effects of collector area on the water temperature in the tank are shown in Fig. 15. The instantaneous water production rates during the operation time are illustrated in Fig. 16. It is obvious that the collector area has a great influence on the performance of the system. Increasing collector area causes significant improvements in water temperature in the tank as well as the instantaneous water production rates. Water temperature with a 5.51 m^2 collector area reaches as high as 77.9 °C at 13:00. With a 1.38 m^2 area, the maximum temperature is only about 53.6 °C at 14:00. As a result, the maximum instantaneous water production rate of the former system is 3.4 times of the latter one.

The variations of *AP*, *SEC*, *COP* and COP_E with varying collector areas are shown in Figs. 17 and 18 respectively. It can be observed that *SEC* is decreased by 16% when the area is increased from 1.38 m^2 to 3.44 m^2. However with the area increasing, the *SEC* increases instead. The reason is that larger collector area means more U-tube evacuated solar collectors. And the latter reason causes a greater fluid pressure drop, which means more electricity consumption for centrifugal pumps. The increase in the accumulated water production becomes slower with the

Table 3
Data and assumptions used in the economic study.

Parameters	Unit	Value
Plant capacity (*AP*)	kg/d	15.85
SEC	kWh/m^3	11.79
Plant availability (*f*) [37]	–	0.9
Plant life (*n*) [37]	Year	20
Interest rate (*i*) [38]	–	5%
Amortization factor (*a*)	–	0.08

Table 4
Cost items for the capital investment, operation and maintenance.

Item	Unitary cost	Quantity	Estimated cost
Direct capital costs			
Fan	27.3 $	1	27.3 $
Pump	28.8 $	3	86.4 $
Dehumidifier	76.0 $	1	76.0 $
Piping and instrumentation	30.4 $	–	30.4 $
Membrane	36 $/m^2	0.59 m^2	21.2 $
Solar collector	120 $/m^2	4.13 m^2	495.6 $
Heat storage tank	1200 $/m^3	0.04 m^3	48.0 $
Total investment (C_{fixed})			784.9 $
Annual fixed charges (A_{fixed})			62.8 $/year
O&M costs			
Electricity cost ($A_{electric}$)	0.136 $/kWh	61.3 kWh/year	8.3 $/year
Membrane replacement ($A_{membrane}$)	20%/year [37]	21.2 $	4.2 $/year
Maintenance cost ($A_{maintenance}$)			12.6 $/year
Annual O&M cost ($A_{O\&M}$)			25.1 $/year
A_{cost}			87.9 $/year
WPC			16.88 $/m^3

area increasing as shown in Fig. 17. Accordingly, the *SEC* has a minimum of 10.8 kWh/m^3 at 3.44 m^2 collector area, when the COP_E reaches a maximum of 63.3 as shown in Fig. 18. This is similar to the tread of the *COP* of the system. When the collector area is larger than 3.44 m^2, the higher water temperature leads to more heat losses from the system to the environment. This is another reason for the decline of the *COP*.

4.5. Economic evaluation

In order to determine the economic feasibility of the proposed solar powered MDHD system, an economic analysis has been made to calculate the final cost for water production (WPC) for the optimized system.

Assuming that the required fund for the system is loaned from the bank, the annual interest payment for capital cost is obtained by multiplying the capital cost by an amortization factor *a*, which is given as:

$$a = \frac{i(1+i)^n}{(1+i)^n - 1} \tag{48}$$

where *i* is the annual interest rate, *n* is the life time of the plant. The values used in Eq. (48) are shown in Table 3. Also listed are other data and assumptions used in the economic study. The operating conditions are a 40 L heat storage tank, with a 4.13 m^2 solar collector area, and a 0.59 m^2 membrane module. Based on these operating conditions, the accumulated water production (*AP*) is 15.85 kg/d. The *SEC* is only 11.79 kWh/m^3, which means that this process is an energy saving alternative to conventional desalination processes such as MSF and RO [35,36]. The electricity rate used here is 0.136 $/kWh, a 2015 market price in Guangzhou.

The annual capital and operating cost (A_{cost}) is the sum of the annual direct capital cost (A_{fixed}) and the annual operating and maintenance cost ($A_{O\&M}$) given as:

$$A_{cost} = A_{fixed} + A_{O\&M} \tag{49}$$

$$A_{fixed} = a \cdot C_{fixed} \tag{50}$$

$$A_{O\&M} = A_{electric} + A_{membrane} + A_{maintenance} \tag{51}$$

$$A_{maintenance} = 0.2A_{fixed} \tag{52}$$

where, C_{fixed} is the total investment of the system. $A_{membrane}$ is annual membrane replacement cost considering the possible effect of bio-fouling in the saline water environment. $A_{electric}$ and $A_{maintenance}$ are annual electricity cost and annual maintenance cost respectively. The WPC of the system can be written as:

$$WPC = \frac{A_{cost}}{(AP \cdot f) \cdot 365} \tag{53}$$

where *f* is the plant availability and can be assumed to be 90% per year [37,38].

C_{fixed}, A_{fixed}, $A_{O\&M}$ and WPC are all listed in Table 4. As seen in Table 4, the solar collector cost contributes to around 63% of the total investment of the system, and the annual operation and maintenance cost is only about 28% of the total water production cost. From Table 4, the final cost for water production is about 16.88 $/m^3, which is comparable to other small-scale renewable energy sources-powered distillation units. The final cost for water production (WPC) is given. The performance is compared to other systems in references as listed in Table 5. Even though the cost for water production is high compared to other industrial scale desalination technology like MSF, whose cost is $2.66/m^3 [41], small membrane-based humidification dehumidification plants like this system are still very attractive because they are flexible due to their modularity and simplicity in operation. This system also provides an alternative desalination system for remote isolated areas as a small-scale, stand-alone system with low maintenance needs. Furthermore, considering the cost of solar collector accounts for most of the total investment, the future development of solar collector technology could reduce the cost of solar collector and ultimately result in reducing the water cost significantly.

5. Conclusions

Feasibility of a solar energy driven and membrane-based air humidification dehumidification desalination (MHDD) system has been studied in this paper. A mathematical model for the whole system is built and validated by experimental data. Both energy and economic analysis are performed to draw following conclusions:

(1) The study confirmed that using hollow fiber membrane module as a humidifier for air humidification is a promising method to provide high purity drinkable water. During the operation time,

Table 5
Final cost for water production (WPC) and comparison of performance with different desalination systems.

Reference	Year	Separation processes	Energy source details	Membrane area (m^2)	Capacity (L/d)	WPC ($/m^3)
[42,43]	1987	Photovoltaic-ED	25 kWp PV	–	10,000	2.38
[39]	1998	Solar energy-MED	38 m^2 solar collector area	–	505	80
[36]	2005	Solar still	3 m^2 effective basin area	–	7.5	50
[36]	2005	Photovoltaic-RO	–	–	17	80
[41]	2006	MSF	Steam and electricity	–	5000	2.66
[37]	2008	Solar energy-MD	5.73 m^2 solar collector area	10	100	15
[37]	2008	Solar energy-MD	72 m^2 solar collector area	40	500	18
[40]	2009	Photovoltaic-solar still	0.15 kWp PV	–	4.6	65.1
[40]	2009	Solar still	1 m^2 effective basin area	–	1.3	39.5
This work	2015	Solar energy-MD	4.13 solar collector area	0.59	15.85	16.88

the electric conductivity of the produced fresh water is less than 12 μS/cm.

(2) The thermal energy storage unit plays an important role to solve the fluctuating nature of solar energy. The system can thus work during weak sunlight hours and even in the night. However for a system with 0.59 m^2 membrane area, there are no benefits to further increase the hot water storage tank above 40 L.

(3) The accumulated water production increases significantly with an increase in solar collector area. The optimum ratio of the storage tank volume to the effective area of solar collector is about 12 L/m^2.

(4) Economic evaluation of the whole system indicates that the system has a low maintenance cost. The water production cost is about 16.88 \$/m^3, which is an acceptable price for a small-scale, stand-alone system to provide clean potable water, especially in remote areas or isolated islands.

Acknowledgements

This Project was supported by the National Science Fund for Distinguished Young Scholars of China, No. 51425601. It was also supported by the Project of National Key Research and Development Program of China, 2016YFB0901404.

References

[1] K.P. Lee, T.C. Arnot, D. Mattia, A review of reverse osmosis membrane materials for desalination—development to date and future potential, J. Membr. Sci. 370 (2011) 1–22.
[2] R. Matz, Z. Zimerman, Low-temperature vapour compression and multi-effect distillation of seawater. Effects of design on operation and economics, Desalination 52 (1985) 201–216.
[3] H. El-Dessouky, H.I. Shaban, H. Al-Ramadan, Steady-state analysis of multi-stage flash desalination process, Desalination 103 (1995) 271–287.
[4] E.S. Mohamed, G. Papadakis, E. Mathioulakis, V. Belessiotis, An experimental comparative study of the technical and economic performance of a small reverse osmosis desalination system equipped with an hydraulic energy recovery unit, Desalination 194 (2006) 239–250.
[5] C.J. Gabelich, M.D. Williams, A. Rahardianto, J.C. Franklin, Y. Cohen, High-recovery reverse osmosis desalination using intermediate chemical demineralization, J. Membr. Sci. 301 (2007) 131–141.
[6] A. Hassan, M. Al-Sofi, A. Al-Amoudi, A. Jamaluddin, A. Farooque, A. Rowaili, A. Dalvi, N. Kither, G. Mustafa, I. Al-Tisan, A new approach to membrane and thermal seawater desalination processes using nanofiltration membranes (part 1), Desalination 118 (1998) 35–51.
[7] J. Ortiz, E. Expósito, F. Gallud, V. García-García, V. Montiel, A. Aldaz, Photovoltaic electrodialysis system for brackish water desalination: modeling of global process, J. Membr. Sci. 274 (2006) 138–149.
[8] F. Banat, N. Jwaied, M. Rommel, J. Koschikowski, M. Wieghaus, Performance evaluation of the "large SMADES" autonomous desalination solar-driven membrane distillation plant in Aqaba, Jordan, Desalination 217 (2007) 17–28.
[9] M.R. Qtaishat, F. Banat, Desalination by solar powered membrane distillation systems, Desalination 308 (2013) 186–197.
[10] H. Geng, H. Wu, P. Li, Q. He, Study on a new air-gap membrane distillation module for desalination, Desalination 334 (2014) 29–38.
[11] S.A. Kalogirou, Seawater desalination using renewable energy sources, Prog. Energy Combust. Sci. 31 (2005) 242–281.
[12] L.F. Greenlee, D.F. Lawler, B.D. Freeman, B. Marrot, P. Moulin, Reverse osmosis desalination: water sources, technology, and today's challenges, Water Res. 43 (2009) 2317–2348.
[13] Y.G. Lee, Y.S. Lee, M. Park, D.R. Yang, J.H. Kim, A fouling model for simulating long-term performance of SWRO desalination process, J. Membr. Sci. 401 (2012) 282–291.
[14] K. Zhani, H.B. Bacha, T. Damak, Modeling and experimental validation of a humidification–dehumidification desalination unit solar part, Energy 36 (2011) 3159–3169.
[15] A. Kabeel, M.H. Hamed, Z. Omara, S. Sharshir, Experimental study of a humidification-dehumidification solar technique by natural and forced air circulation, Energy 68 (2014) 218–228.
[16] S. Farsad, A. Behzadmehr, Analysis of a solar desalination unit with humidification–dehumidification cycle using DoE method, Desalination 278 (2011) 70–76.
[17] F.A. Al-Sulaiman, M.I. Zubair, M. Atif, P. Gandhidasan, S.A. Al-Dini, M.A. Antar, Humidification dehumidification desalination system using parabolic trough solar air collector, Appl. Therm. Eng. 75 (2015) 809–816.
[18] K. Zhani, H.B. Bacha, Experimental investigation of a new solar desalination prototype using the humidification dehumidification principle, Renew. Energy 35 (2010) 2610–2617.
[19] J. Navarrete-Gonzalez, J. Cervantes-de Gortari, E. Torres-Reyes, Exergy analysis of a rock bed thermal storage system, Int. J. Exergy 5 (2008) 18–30.
[20] K. Çomaklı, U. Çakır, M. Kaya, K. Bakirci, The relation of collector and storage tank size in solar heating systems, Energy Convers. Manag. 63 (2012) 112–117.
[21] L.-Z. Zhang, S.-M. Huang, Coupled heat and mass transfer in a counter flow hollow fiber membrane module for air humidification, Int. J. Heat Mass Transf. 54 (2011) 1055–1063.
[22] Y. Kim, T. Seo, Thermal performances comparisons of the glass evacuated tube solar collectors with shapes of absorber tube, Renew. Energy 32 (2007) 772–795.
[23] L.-Z. Zhang, Coupled heat and mass transfer in an application-scale cross-flow hollow fiber membrane module for air humidification, Int. J. Heat Mass Transf. 55 (2012) 5861–5869.
[24] J.A. Duffie, W.A. Beckman, Solar Energy Thermal Processes, University of Wisconsin-Madison, Solar Energy Laboratory, Madison, WI, 1974.
[25] L. Ma, Z. Lu, J. Zhang, R. Liang, Thermal performance analysis of the glass evacuated tube solar collector with U-tube, Build. Environ. 45 (2010) 1959–1967.
[26] T.L. Bergman, F.P. Incropera, A.S. Lavine, Fundamentals of Heat and Mass Transfer, John Wiley & Sons, 2011.
[27] L.Z. Zhang, Conjugate Heat and Mass Transfer in Heat Mass Exchanger Ducts, Elsevier, 2013.
[28] C.J. Simonson, R.W. Besant, Energy wheel effectiveness: part I—development of dimensionless groups, Int. J. Heat Mass Transf. 42 (1999) 2161–2170.
[29] L. Zhang, Energy performance of independent air dehumidification systems with energy recovery measures, Energy 31 (2006) 1228–1242.
[30] V. Gnielinski, New equations for heat and mass transfer in turbulent pipe and channel flows, Int. Chem. Eng. 16 (1976) 359–368.
[31] C.-C. Wang, Y.-c. Hsieh, Y.-t. Lin, Performance of plate finned tube heat exchangers under dehumidifying conditions, J. Heat Transf. 119 (1997) 109–117.
[32] G.P. Li, L.Z. Zhang, Investigation of a solar energy driven and hollow fiber membrane-based humidification–dehumidification desalination system, Appl. Energy 177 (2016) 393–408.
[33] J. Huang, S. Pu, W. Gao, Y. Que, Experimental investigation on thermal performance of thermosyphon flat-plate solar water heater with a mantle heat exchanger, Energy 35 (2010) 3563–3568.
[34] I. Budihardjo, G. Morrison, Performance of water-in-glass evacuated tube solar water heaters, Sol. Energy 83 (2009) 49–56.
[35] M. Darwish, N.M. Al-Najem, Energy consumption by multi-stage flash and reverse osmosis desalters, Appl. Therm. Eng. 20 (2000) 399–416.
[36] S. Bouguecha, B. Hamrouni, M. Dhahbi, Small scale desalination pilots powered by renewable energy sources: case studies, Desalination 183 (2005) 151–165.
[37] F. Banat, N. Jwaied, Economic evaluation of desalination by small-scale autonomous solar-powered membrane distillation units, Desalination 220 (2008) 566–573.
[38] S. Al-Obaidani, E. Curcio, F. Macedonio, G. Di Profio, H. Al-Hinai, E. Drioli, Potential of membrane distillation in seawater desalination: thermal efficiency, sensitivity study and cost estimation, J. Membr. Sci. 323 (2008) 85–98.
[39] H. Müller-Holst, M. Engelhardt, M. Herve, Solarthermal seawater desalination systems for decentralised use, Renew. Energy 14 (1998) 311–318.
[40] S. Kumar, G.N. Tiwari, Life cycle cost analysis of single slope hybrid (PV/T) active solar still, Appl. Energy 86 (2009) 1995–2004.
[41] A.S. Nafey, H.E.S. Fath, A.A. Mabrouk, Thermo-economic investigation of multi effect evaporation (MEE) and hybrid multi effect evaporation-multi stage flash (MEE-MSF) systems, Desalination 201 (2006) 241–254.
[42] O. Kuroda, S. Takahashi, K. Wakamatsu, An electrodialysis sea water desalination system powered by photovoltaic cells, Desalination 65 (1987) 161–169.
[43] M.T. Ali, H.E.S. Fath, P.R. Armstrong, A comprehensive techno-economical review of indirect solar desalination, Renew. Sust. Energ. Rev. 15 (2011) 4187–4199.

Nomenclature

a amortization factor:
A_a outer surface area of absorber tubes (m^2):
A_{cost} Annual capital and operating cost:
A_e effective heat absorption area of absorber tubes (m^2):
A_p the projection area of absorber tubes (m^2):
A_v packing density (m^2/m^3):
c_{pa} specific heat of air (kJ/kg K^{-1}):
c_{ps} specific heat of solution (kJ/kg K^{-1}):
d/D diameter (m):
D_h hydraulic diameter (m):
D_{vm} moisture diffusivity in membrane (m^2/s):
f friction factor, plant availability:
F_R the collector heat removal factor:
H enthalpy (kJ/kg), height (m):
H_w latent heat of water evaporation (kJ/kg):
h convective heat transfer coefficient (kW m^{-2} K^{-1}):
i the annual interest rate:
I_t the global solar radiation (W/m^2):
J Colburn j factor:
k convective mass transfer coefficient (m/s):
l/L length (m):
Le Lewis number:
m mass flow rate (kg/s):
n the life time of the plant (year):
n_{col} number of solar collector tubes:
n_f number of fibers:
N_L number of fibers along air flow direction:

N_r number of tube row:
NTU Number of Transfer Units:
Nu Nusselt number:
P pressure (Pa):
P_F Fin pitch (mm):
P_L Longitudinal pitch (mm).:
P_T Transverse pitch (mm):
Pr Prandtl number:
q heat transfer rate (kW):
Re Reynolds number:
RH relative humidity (%):
R_w thermal conduction resistance (K/W):
Sh Sherwood number:
T temperature (K):
U heat transfer coefficient ($W\,m^{-2}\,K^{-1}$):
U_L the collector overall loss coefficient ($W\,m^{-2}\,K^{-1}$):
u velocity (m/s):
V specific volume (m^3/kg):
W width (m), power (kW):
X solution concentration (%):
x spatial coordinate (m):
y spatial coordinate (m):

Greek letters

α absorptivity of the selective absorbing coating:
δ thickness (m):
ε effectiveness:
Φ packing fraction:
η_i instantaneous collector efficiency:
η_o: fin efficiency
λ heat conductivity ($Wm^{-1}\,K^{-1}$):
λ_E electric conductivity (μS/cm):
ν kinematic viscosity (m^2/s):
ρ density (kg/m^3):
τ transmissivity of the outer glass:
ω humidity (kg/kg):
Π_c wet perimeter of channel (m):

Subscripts

a air:
c cold side, channel:
coil coil heat exchanger in the heat storage tank:
Cal calculated:
D dehumidifier:
e environment:
E electrical:
f distilled water in the collector tube:
fan fan:
fin aluminum fins in the dehumidifier:
h shot side:
H humidifier:
i inlet, inner:
m membrane:
max maximum value:
min minimum value:
o outlet, outer:
O&M operation and maintenance.:
p the absorber tube.:
pump. pump.:
real. real.:
s solution:
solar solar energy:
t heat storage tank:
tot total:
test tested:
w water: